Bio-Design and Manufacturing (2024) 7:262–276
https://doi.org/10.1007/s42242-024-00272-8

RESEARCH ARTICLE

Development and characterization of 3D-printed electroconductive pHEMA-co-MAA NP-laden hydrogels for tissue engineering

Sara De Nitto[1] · Aleksandra Serafin[2,4] · Alexandra Karadimou[2] · Achim Schmalenberger[3] · John J. E. Mulvihill[2] · Maurice N. Collins[2,4,5]

Received: 10 August 2023 / Accepted: 26 February 2024 / Published online: 25 April 2024

Abstract

Tissue engineering (TE) continues to be widely explored as a potential solution to meet critical clinical needs for diseased tissue replacement and tissue regeneration. In this study, we developed a poly(2-hydroxyethyl methacrylate-co-methacrylic acid) (pHEMA-co-MAA) based hydrogel loaded with newly synthesized conductive poly(3,4-ethylene-dioxythiophene) (PEDOT) and polypyrrole (PPy) nanoparticles (NPs), and subsequently processed these hydrogels into tissue engineered constructs via three-dimensional (3D) printing. The presence of the NPs was critical as they altered the rheological properties during printing. However, all samples exhibited suitable shear thinning properties, allowing for the development of an optimized processing window for 3D printing. Samples were 3D printed into pre-determined disk-shaped configurations of 2 and 10 mm in height and diameter, respectively. We observed that the NPs disrupted the gel crosslinking efficiencies, leading to shorter degradation times and compressive mechanical properties ranging between 450 and 550 kPa. The conductivity of the printed hydrogels increased along with the NP concentration to $(5.10\pm0.37)\times10^{-7}$ S/cm. In vitro studies with cortical astrocyte cell cultures demonstrated that exposure to the pHEMA-co-MAA NP hydrogels yielded high cellular viability and proliferation rates. Finally, hydrogel antimicrobial studies with staphylococcus epidermidis bacteria revealed that the developed hydrogels affected bacterial growth. Taken together, these materials show promise for various TE strategies.

✉ Maurice N. Collins
Maurice.Collins@ul.ie

1 DIBRIS Polytechnic Inter-School Section, University of Genoa, 16126 Genoa, Italy

2 School of Engineering, Bernal Institute, University of Limerick, Limerick V94 T9PX, Ireland

3 School of Natural Sciences, Department of Biological Sciences, University of Limerick, Limerick V94 T9PX, Ireland

4 Health Research Institute, University of Limerick, Limerick V94 T9PX, Ireland

5 AMBER, University of Limerick, Limerick V94 T9PX, Ireland

Graphic abstract

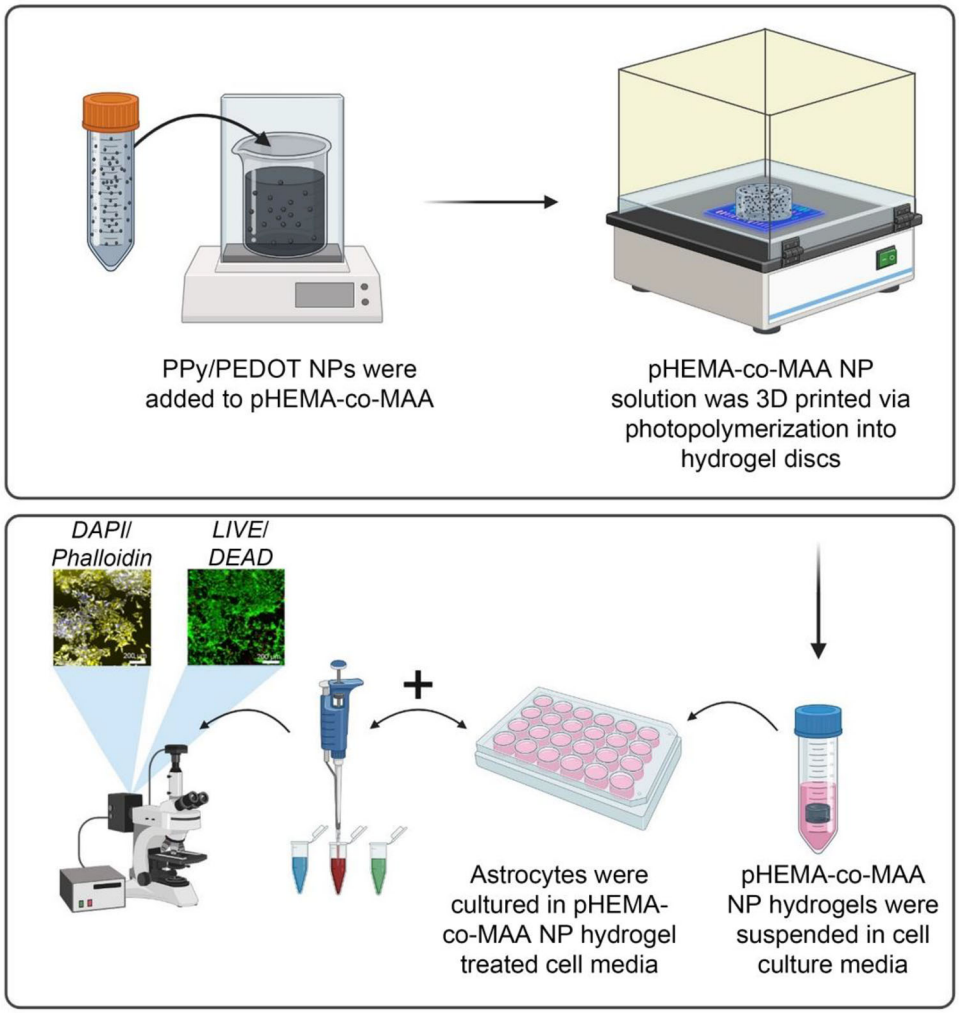

Keywords Conductive nanoparticles · Hydroxyethyl methacrylate (HEMA) · Ultraviolet (UV) polymerization · 3D printing

Introduction

Transplantation is the traditional treatment approach in the case of partial or complete loss of the functionality of one or more organs, offering critically ill patients an improvement in the quality of life. However, this method also displays substantial problems, notably in difficulty in procuring suitable donors and the risk of immunorejection [1].

Such issues have opened new horizons for regenerative medicine, with tissue engineering (TE) strategies showing potential. Appropriate material selection is central to TE, as materials interact with biological systems to influence, replace, or restore the missing function [2], e.g., by mimicking the extracellular matrix (ECM) of the native tissue to provide cell growth and proliferation support, ultimately resulting in tissue regeneration.

Among the suitable materials for biomimetic matrix development that replicate the complex micro-geometry and three-dimensionality of the in vivo extracellular environment, hydrogels are taking on an ever-increasing role [3]. Hydrogels are three-dimensional (3D) hydrophilic networks of water-soluble polymers, which can be transformed into insoluble compounds upon photopolymerization. Hydrogels were first applied in the medical field upon the introduction of photopolymerized poly(hydroxyethyl methacrylate) (pHEMA) hydrophilic matrices [4]. pHEMA exhibits limited oxygen transmission due to its low water content of approximately 38% [5]. To increase their water content, hydrogels are often supplemented with methacrylic acid (MAA) or N-vinyl pyrrolidone (NVP), generating etafilcon A and nesofilcon A, respectively. The most prominent applications of pHEMA-based materials are their use in contact

lenses [6], drug delivery applications [2], and implantation strategies due to their lack of toxicity and high degradation resistance [7].

Several factors make 3D printing (or additive manufacturing) one of the most common scaffold-producing methods for TE applications [8–11]. Their most important advantage is the precision of the instrumentation, allowing to develop intricate and complex geometries for customized organ and tissue production. In addition, 3D printing enables large-scale production allowing for faster turnover and response to clinical needs, lower energy consumption and costs (hence lower prices), and reduced carbon emissions, thereby representing an ecologically more sustainable approach [12].

The material features of a suitable 3D printing candidate depend on specific applications. For example, in permanent bone implants, certain hardness and impact resistance are required. In drug delivery applications, the material must degrade in a specific manner, and in the case of skin applications, material flexibility and toughness are pivotal.

When examining cells and tissues in situ, another considerable characteristic is electrical stimulation, which allows tissues to promote and control growth as well as remodel and absorb proteins [7, 13, 14]. For example, electrically active materials reportedly enhanced neurite extension in vitro and the growth directionality of cells could also be controlled [15]. Furthermore, the application of a current mimicking the native electrophysiological environment in cell cultures has been used in TE investigations combined with electroconductive scaffolds [16]. Element supplementation, such as that of carbon nanotubes (CNTs) [17, 18], carbon nanofibers (CNFs) [19], or conductive polymers [20, 21], could raise biomaterial scaffold conductivity. However, major drawbacks of using carbon additives or conductive polymers could arise from low conductivity under neutral pH, insolubility in water, and poor biofunctionality or biocompatibility, factors which severely limit their successful use in in vivo applications [22–26].

In this study, we prepared the 3D printed and electroconductive pHEMA-co-MAA hydrogel-based scaffold prototypes laden with two conductive nanoparticle (NP) types, poly(3,4-ethylene-dioxythiophene) (PEDOT) and polypyrrole (PPy), previously synthesized by our research group [7, 20, 27]. The advantage of these NPs over commercially available conductive polymers, such as PEDOT:poly(styrene sulfonate) (PEDOT:PSS), arises from the lack of reliance on additives with poor biofunctionality/biocompatibility to induce conductivity [23, 28]. In addition, the NP synthesis method could easily be altered to change NP surface functionalization by modifying the surfactant used during the synthesis, e.g., by utilizing hyaluronic acid to target specific cell interactions.

We produced the pHEMA-co-MAA NP hydrogels via in situ monomer mixture photopolymerization during 3D printing. To determine how the material structure/property influenced the processing/function relationships of these biomaterials, we fully characterized them chemically, structurally, morphologically, and rheologically, and assessed them as bioinks in 3D printing trials. Furthermore, we performed cell viability and antimicrobial assessments in vitro. Taken together, the hydrogel system we developed in this study exhibits promising potential for antimicrobial applications (e.g., patches for wound healing assessment), biological sensor production, and peripheral nerve repair.

Materials and methods

Materials

Hydroxyethyl methacrylate (HEMA), methacrylic acid, Iragcure 2959, 3,4-ethylenedioxythiophene (EDOT), pyrrole, poly(diallyldimethylammonium chloride) (PDADMAC) solution, iron(III) p-toluenesulfonate hexahydrate (Fe-Tos), and 30% (mass fraction) hydrogen peroxide (H_2O_2) were purchased from Sigma-Aldrich, Ireland.

For cell culture experiments, we used DI TNC1 cells, an SV40 immortalized rat astrocyte cell line, purchased from LCG (ATCC-CRL-2005), to study how the hydrogels and NPs could affect cell viability. We used Dulbecco's modified minimal essential medium (DMEM) (Sigma Aldrich D6546) supplemented with 10% fetal bovine serum (Sigma Aldrich F7524), 4 mmol/L L-Glutamine (Sigma Aldrich G7513), 2 mmol/L sodium pyruvate (Sigma Aldrich S8636), 100 U/mL penicillin, and 100 μg/mL streptomycin (Sigma Aldrich P4333) to culture the cells at 37 °C in an atmosphere of 5% CO_2.

Upon reaching confluency, we detached the cells using a 0.25% trypsin–EDTA solution (Sigma Aldrich T4049) and resuspended them in a DI TNC1 cell culture medium at a concentration of 1×10^6 cells/mL. All experiments were conducted using cell passages of 23–24.

For antimicrobial testing, tryptic soy broth (TSB) and *Staphylococcus epidermidis* bacteria DSM 28319 were purchased from Sigma Aldrich (Ireland) and DSM (Germany), respectively.

Nanoparticle synthesis

We synthesized the NPs by chemical oxidation polymerization in mini-emulsion (Fig. 1) as described previously [7, 20, 27, 29]. Briefly, 0.037 mol/L of pyrrole/EDOT monomer was added into an aqueous PDADMAC (surfactant) solution. The solution was stirred and subsequently ultrasonicated for 10 min, while cooling it in an ice-water bath to obtain a mini-emulsion. We supplemented the mini-emulsion with 0.056 mol/L of Fe-Tos solution in deionized (DI) water in a dropwise manner under constant stirring at 45 °C, then

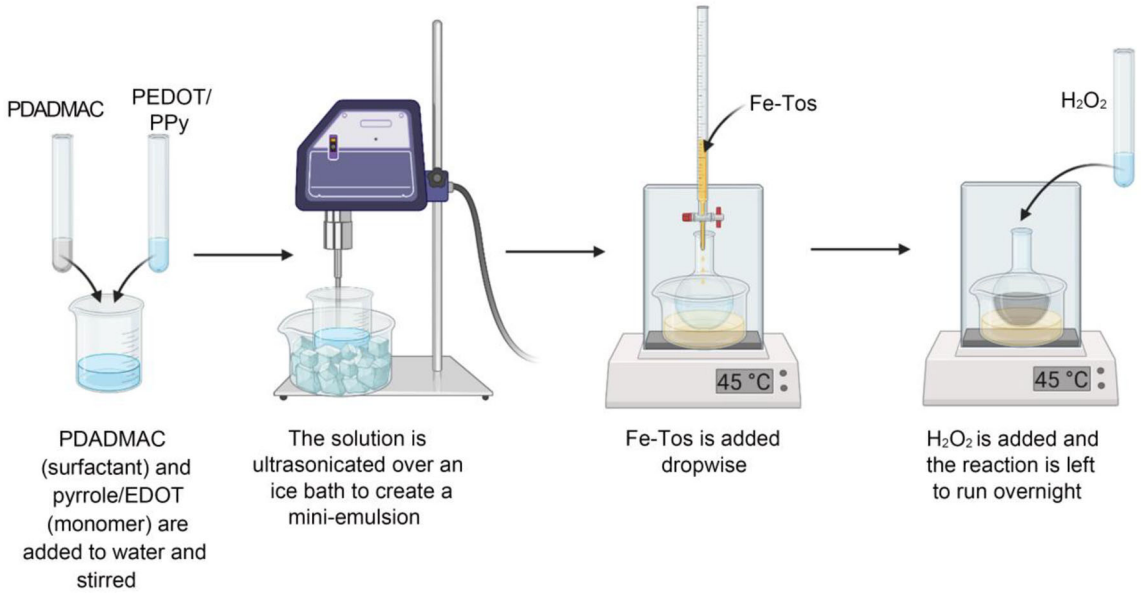

Fig. 1 Schematic of nanoparticle synthesis. PDADMAC: poly(diallyldimethylammonium chloride); PEDOT: poly(3,4-ethylene-dioxythiophene); PPy: polypyrrole; EDOT: 3,4-ethylenedioxythiophene; Fe-Tos: iron(III) p-toluenesulfonate hexahydrate

added 0.001 mol/L of H_2O_2 to the reaction and incubated it overnight. Finally, we purified the NPs by centrifugation at 8500 r/min for 20 min three times, with a final redispersion in 40 mL of DI water.

pHEMA-co- MAA NP sample preparation

To prepare the pHEMA-co-MAA NP solutions, we first added 3% (mass fraction) MAA to HEMA under continuous stirring for 5 min, followed by supplementing the monomer mix with 1% (mass fraction) Iragcure 2959. NPs were then dispersed in an adequate volume of the mixture (Table 1). We mixed the monomer-NP solutions until complete NP dispersion with no visible residues. The solutions were covered with foil and stored far from direct light.

3D-printed pHEMA-co-MAA NP solution in situ photopolymerization

The pHEMA-co-MAA NP samples were in situ photopolymerized, converting 3D printed layers of the monomer solutions laden with NPs to hydrogels using an Anysubic Photon S, a liquid–crystal display (LCD)-based stereolithography (SLA) 3D printer with an ultraviolet (UV) light of wavelength of 405 nm. We created cylinder models 2 mm in height and 10 mm in diameter using the Chitubox software (China, 2014). The printing was done by slicing the 3D model with a printing speed of approximately 20 mm/h. The exposure time of the samples to the NPs was 70 s for each layer.

pHEMA-co-MAA NP sample characterization

UV–Vis spectrophotometry was performed with the Carry 4000 UV–Vis spectrophotometer. The absorbance of the NPs was analyzed with wavelengths from 300 to 800 nm.

Rheological tests were conducted with a hybrid rheometer (TA Instruments, USA), with a UV light lamp to replicate photopolymerization in the 3D printer. Briefly, disposable 25 mm aluminum rheological plates were used for the analysis with a measurement gap of 550 μm. The pHEMA-co-MAA NP samples were tested using the following regimes: (1) frequency sweeps of 0.1–100 rad/s at a constant strain of 2%; (2) UV light wavelength of 365 nm at 350 $\mu W/cm^2$, with frequency sweep of 10 rad/s at the determined constant strain of 5%.

Compression tests were conducted on the NP hydrogels using an in-house compression test facility equipped with a 1-kN load cell at a compression rate of 1 mm/s between parallel plates. Young's moduli of samples were calculated as the linear region slope of a normalized stress vs. strain graph.

Resistivity measurements were conducted with an Ohm meter using the two-probe method. Conductivity of the samples was then calculated by means of Pouillet's law as follows:

$$\sigma = \frac{l}{RA}, \tag{1}$$

where σ, l, A, and R label the conductivity, sample length, cross-section area, and resistance, respectively.

Table 1 pHEMA-co-MAA conductive hydrogel composition

Sample name	HEMA/MAA/Iragcure 2959 (mL)	NP concentration (mg/mL)	
		PEDOT NPs	PPy NPs
0.25×	40	1.95	1.72
0.33×	30	2.57	2.27
0.5×	20	3.90	3.44
1×	10	7.80	6.88

pHEMA-co-MAA: poly(2-hydroxyethyl methacrylate-co-methacrylic acid); HEMA: hydroxyethyl methacrylate; MAA: methacrylic acid; NP: nanoparticle; PEDOT: poly(3,4-ethylene-dioxythiophene); PPy: polypyrrole

Swelling tests were conducted by initially drying the samples for five days under vacuum at 80 °C, with the dry mass of the prepared samples recorded. At time $t = 0$ s the samples were immersed in DI water and placed inside an incubator at 37 °C for 96 h. The wet mass of the samples was then recorded at specified time points, with the swelling degree calculated as follows:

$$S = \left(\frac{W_s - W_d}{W_d}\right) \times 100\%, \quad (2)$$

where W_s and W_d represent the hydrogel swollen mass and dried mass measured at the beginning of the test, respectively.

Fourier transform infrared spectroscopy (FTIR) spectra of the printed pHEMA-co-MAA NP-laden hydrogels were analyzed with a spectrum 100 FTIR (PerkinElmer, USA) in the range of 650–4000 cm^{-1} for 10 scans.

Morphological analysis was conducted via scanning electron microscope (SEM) (Hitachi TM-1000) tabletop microscope. Prior to analysis, samples were lyophilised at −50 °C with no drastic change in their shape or size and were subsequently sputtered with gold.

pHEMA-co-MAA NP-laden hydrogel cytocompatibility assessment in vitro

To assess the biological responses to the pHEMA-co-MAA NP-laden hydrogels, three tests were conducted on astrocyte cell cultures (Fig. 2). For all biological tests, the DI TNC1 cell cultures were seeded at a density of 5×10^3 cells/well in 24-well plates and allowed to attach overnight, followed by supplementation with 1 mL of NP hydrogel-treated cell culture media.

LIVE/DEAD staining of the astrocytes was conducted after 96 h by means of Calcein AM and propidium iodine. Morphological assessment of the cells was also conducted after 96 h in culture. The cells were first fixed with 4% paraformaldehyde (PFA), stained with 4',6-diamidino-2-phenylindole (DAPI) (1:2000, D9542-10MG) and phalloidin (1:400), and imaged using an ImageXpress confocal microscope for fluorescence imaging (Molecular Devices, USA). The cell viability was then quantitatively analyzed using ImageJ. Moreover, pHEMA-co-MAA NP samples were tested for potential cytotoxicity by means of the Alamar Blue proliferation assay. Alamar Blue was added to the wells at 10% of the well volume and incubated for 5 h. Measurement of the cell fluorescent emission was carried out using SynergyMx (BioTek, UK) at a wavelength of 545/590 nm, following the manufacturer's protocol.

PHEMA-CO-MAA NP sample antimicrobial assessment

pHEMA-co-MAA NP samples were tested for potential antimicrobial properties by the direct contact assay method as previously described [30] with modifications. Briefly, we cultured *S. epidermidis* DSM 28319 (DSM, Germany) in TSB until reaching a concentration of 8×10^7 bacterial cells/mL, calculated by serial dilution and enumeration. pHEMA-co-MAA NP samples were 3D-printed as described above, sterilized with UV light, washed with 25% ethanol thrice, and subsequently inoculated with 20 μL of bacterial suspension (1.6×10^6 cells) in triplicates. Samples were incubated at 30 °C for 24 h, followed by 2 mL of 10% TSB medium supplementation. The samples were incubated in a rotating incubator (Innova42, Brunswick Scientific, USA) at 30 °C for 72 h at 30 r/min to assess cell viability and growth inhibition upon direct contact with the pHEMA-co-MAA NP-laden hydrogels. Measurement of the bacterial optical density (OD) from the planktonic phase was taken by means of microtiter plate reading at 600 nm using an Eon plate reader (BioTek, UK). The optical density of the background of the growth media was subtracted from the individual sample readings.

Statistical analysis

To highlight the significant difference between the populations, the chosen statistical analysis was a two tailed unpaired *t*-test with a *p*-value of <0.05 considered as statistically significant ($^*p<0.05$). A Gaussian distribution of the data was assumed, and a parametric *t*-test was considered. Moreover,

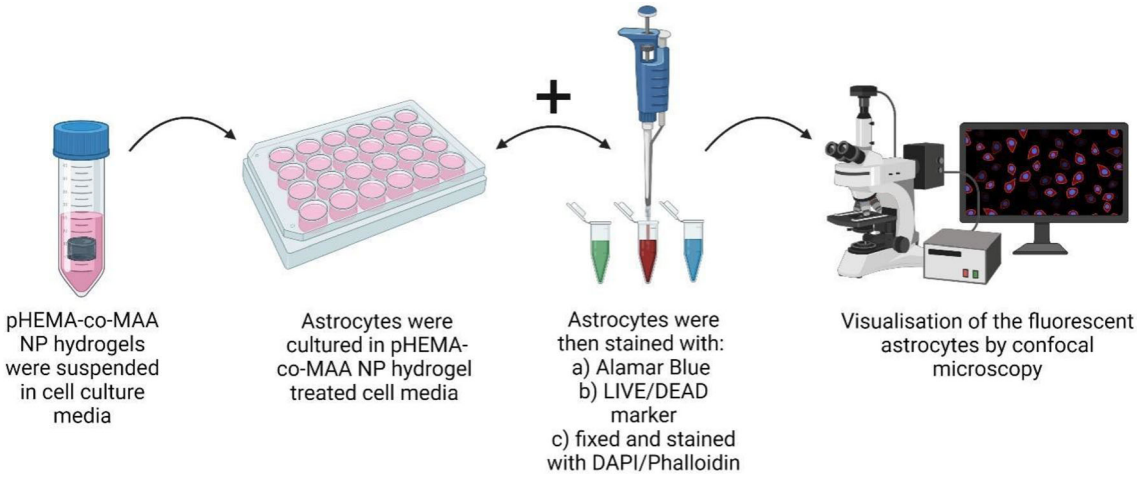

Fig. 2 Schematic of pHEMA-co-MAA NP hydrogel biocompatibility testing in vitro using the indirect contact assay. pHEMA-co-MAA: poly(2-hydroxyethyl methacrylate-co-methacrylic acid); NP: nanoparticle; DAPI: 4',6-diamidino-2-phenylindole

we assumed identical standard deviations for both populations and that Welch's correction was not necessary. For the cellular analysis, experiments were conducted in triplicates, with the data presented as mean±standard deviation. To determine the statistical significance, one-way analysis of variance (ANOVA) was employed with the p-value of <0.05 considered as statistically significant ($^{*}p<0.05$). A two-way ANOVA was employed for the Alamar Blue cytocompatibility analysis and the antimicrobial analysis, with the p-value of <0.05 considered as statistically significant ($^{*}p<0.05$).

Results and discussion

pHEMA-co-MAA NP-laden hydrogel UV–Vis assessment

The UV–Vis characterization of the PEDOT and PPy NPs yielded a higher absorbance measurement for the PPy NP than for the PEDOT NP solution (0.4±0.04 and 0.3±0.07, respectively). This implies that the PPy solution is less transparent than the PEDOT solution, thus enabling higher UV transmission in the PEDOT samples, resulting in more tightly crosslinked hydrogel networks (Fig. 3).

pHEMA-co-MAA NP-laden hydrogel rheological assessment

Rheological analysis of the NP-laden pHEMA-co-MAA monomer mix conversion to a hydrogel under UV light was assessed to determine its suitability for printing and to determine a 3D printing processing window. The storage moduli and the loss moduli of the NP-laden pHEMA-co-MAA monomer mix were studied over a constant angular velocity when subjected to UV light (Figs. 4a and 4b). We observed that both the storage and loss moduli increased with increasing UV exposure, with the loss modulus overtaking the storage modulus, indicating the crosslinking onset. The lower the concentration of the NPs, the more evident this phenomenon is. This was particularly apparent in the case of the 1× PEDOT sample, which displayed no increase in either moduli during the observation period. This is potentially due to the presence of the blue/black NPs across the narrow passage between the rheometer plates which block the UV light transmission into the hydrogel matrix, as further indicated by the UV–Vis study. Figure 4c shows the rheological analysis of the NP-laden pHEMA-co-MAA monomer mix conversion into a hydrogel under UV light, monitored in terms of complex viscosity changes, which highlights that the PEDOT 0.25× and 1× samples (with the lowest and highest NP concentrations, respectively) exhibited complex viscosities of 2356.8 and 0.09 Pa·s, respectively. We also observed the same trend for monomers laden with PPy NPs with the PPy 0.25× and 1× samples displaying complex viscosities of 822.1 and 0.05 Pa·s, respectively. Therefore, the PEDOT 1×, PPy 0.5×, and PPy 1× viscosities remained constant during the 2 h observation period, implying impeded crosslinking, potentially due to insufficient UV transmission into the samples within the rheological assessment setup. The control (without NPs) reached the highest complex viscosity (17,073.7 Pa·s) after 2 h of direct exposure, implying undisrupted gelation (i.e., crosslinking).

pHEMA-co-MAA NP-laden hydrogel 3D printing

Table 2 summarizes the examples of 3D printed pHEMA-co-MAA NP-laden hydrogels. The printed shapes for the control

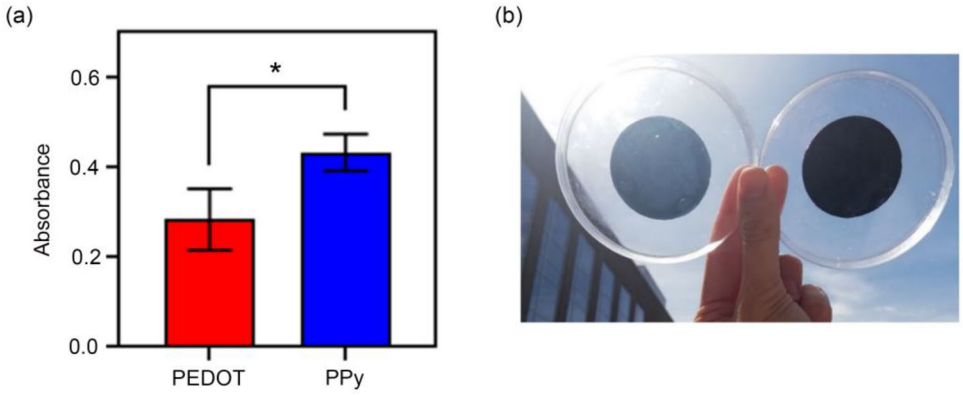

Fig. 3 **a** PEDOT and PPy NP UV–Vis analyses; $^{*}p<0.05$ ($n=3$, mean±SD). **b** Comparison between representative PEDOT and PPy pHEMA-co-MAA NP sample transparencies against natural light. PEDOT: poly(3,4-ethylene-dioxythiophene); PPy: polypyrrole; NP: nanoparticle; UV–Vis: ultraviolet–visible; SD: standard deviation; pHEMA-co-MAA: poly(2-hydroxyethyl methacrylate-co-methacrylic acid)

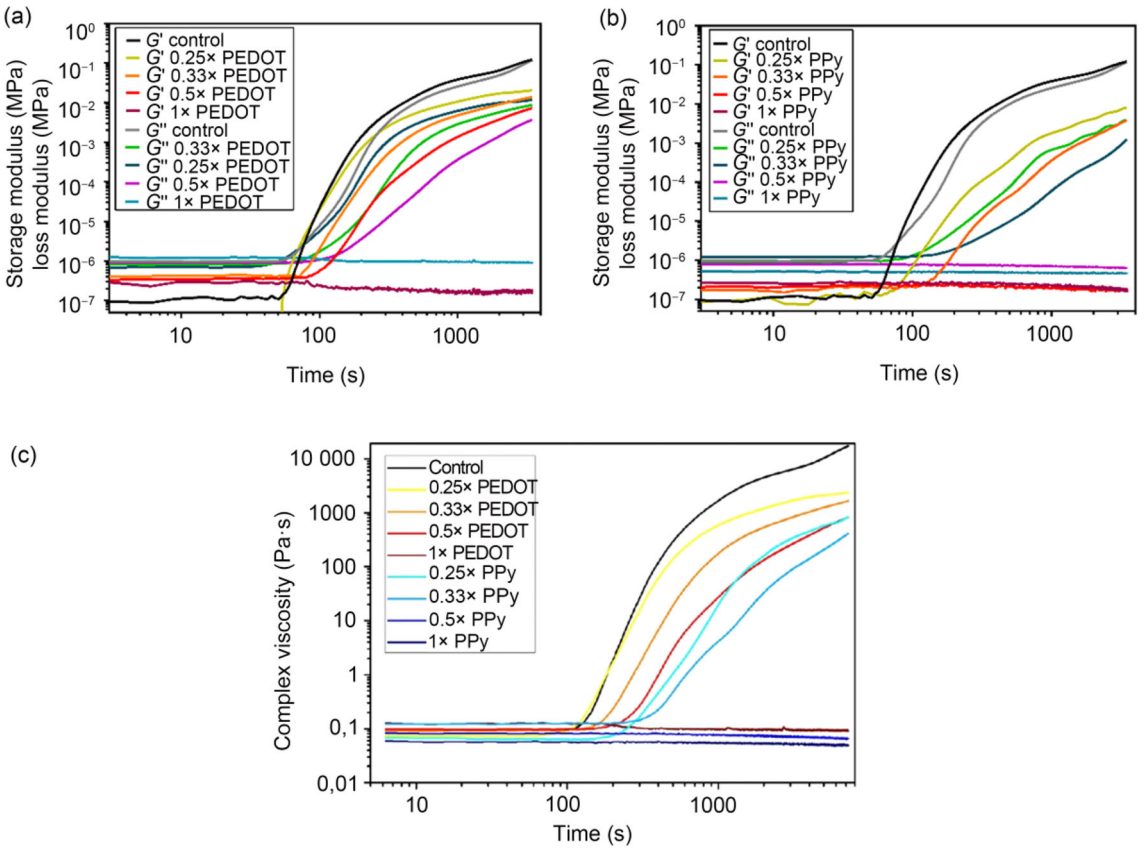

Fig. 4 **a**, **b** pHEMA-co-MAA NP hydrogel storage and loss moduli when subjected to UV light. **c** pHEMA-co-MAA NP hydrogel viscosities when subjected to UV light. pHEMA-co-MAA: poly(2-hydroxyethyl methacrylate-co-methacrylic acid); NP: nanoparticle; UV: ultraviolet; PEDOT: poly(3,4-ethylene-dioxythiophene); PPy: polypyrrole

and PEDOT/PPy NP samples were consistent with the Chitubox model. The control required less exposure time than the pHEMA-co-MAA NP-laden hydrogels (25 s vs. 70 s) due to the unrestricted gelation. The printing variances between the two NP-laden hydrogels were attributed to their different transparencies (Fig. 3a). UV light could penetrate the PEDOT solution more easily than the PPy solution, allowing for more efficient crosslinking of printed hydrogels, which was also observed during the rheological analysis (Fig. 4). Higher NP concentrations yielded poorer print quality, with the PPy 1× sample being unsuitable for printing. Lower NP concentrations provided better print fidelity.

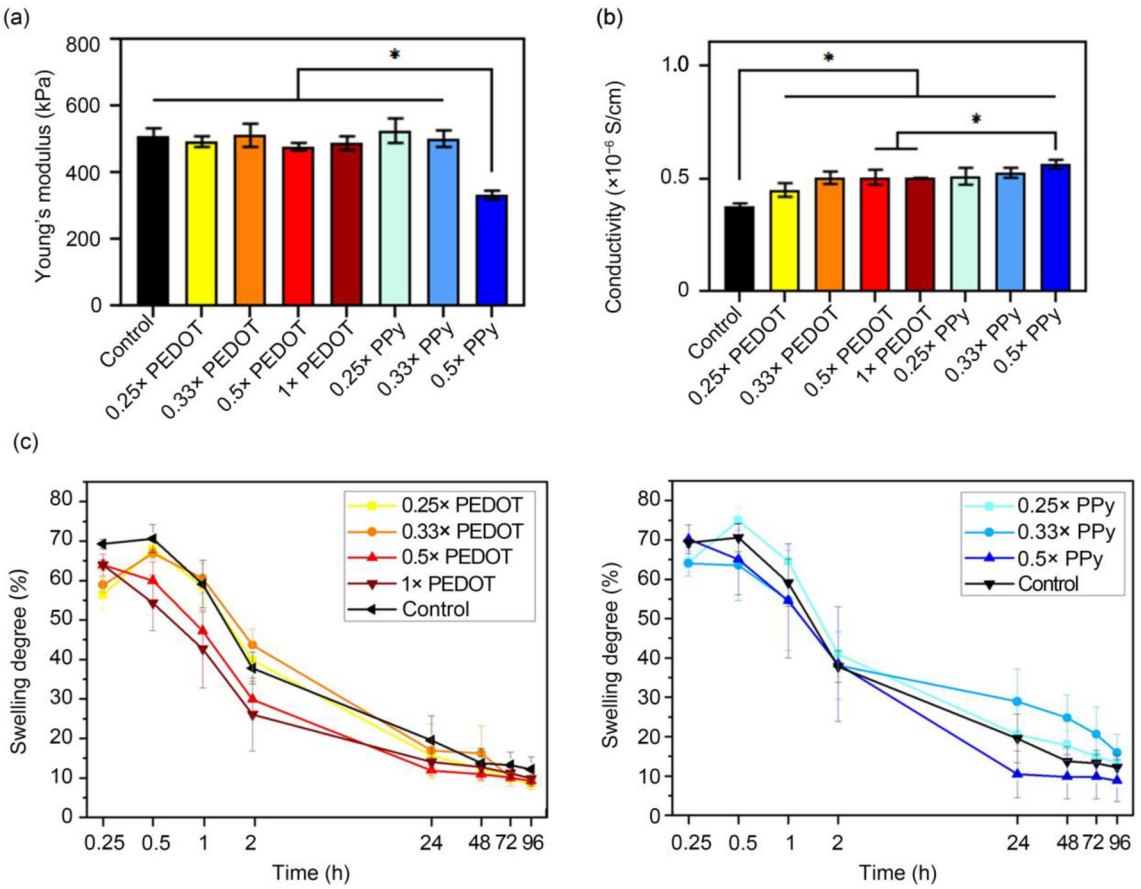

Fig. 5 **a** Young's moduli and **b** conductivities of the pHEMA-co-MAA NP samples; $^{*}p<0.05$ (n=3, mean±SD). **c** Swelling profiles of pHEMA-co-MAA PEDOT NP samples (left) and pHEMA-co-MAA PPy NP samples (right) over a 96 h observation period. pHEMA-co-MAA: poly(2-hydroxyethyl methacrylate-co-methacrylic acid); NP: nanoparticle; SD: standard deviation; PEDOT: poly(3,4-ethylene-dioxythiophene); PPy: polypyrrole

pHEMA-co-MAA NP-laden hydrogel mechanical properties

Analysis of the mechanical properties of the pHEMA-co-MAA NP-laden hydrogel (Fig. 5) showed that the Young's moduli remained between (478.1±9.9) and (526.4±30.3) kPa with increasing NP concentrations, except for the PPy 0.5× hydrogel (Fig. 5a). The PEDOT and PPy samples did not display significant differences in terms of mechanical performance, (e.g., PEDOT 0.25× and PPy 0.25× exhibited Young's moduli of (493.0±13.2) and (526.4±30.3) kPa, respectively). However, PPy 0.5× yielded a significantly lower value ((333.1±11.1) kPa), consistent with the rheological test (Fig. 4). PPy NPs seemed to block UV rays, thereby lowering the crosslinking efficiency and Young's modulus.

In comparison, pHEMA has also been previously combined with pyrrole for cryogel development, yielding a Young's modulus of (1.45±0.21) MPa [31]. Moreover, pHEMA was combined with 1%–6% (mass fraction) multiwalled CNT for nerve conduit development to repair peripheral nerve injury, resulting in a Young's modulus of (0.41±0.05) MPa [32]. The Young's modulus values presented in this study are similar to those in the human nervous tissue (approximately 200–500 kPa) [7], pathological human heart (beyond 100 kPa) [33], and kidney tissue (approximately 200 kPa) [34], highlighting their potential to be used for mechanically biomimetic TE approaches.

pHEMA-co-MAA NP-laden hydrogel conductive properties

Overall, the results of the electrical conductivity analysis indicated that NP supplementation increased hydrogel system conductivities (Fig. 5b). The electroconductivity values of the printed samples with NPs remained below (4.5±0.3)×10^{-7} and (5.10±0.37)×10^{-7} S/cm for the PEDOT and PPy NP samples, respectively, while that of the control was (3.8±0.1)×10^{-7} S/cm. Although the conductivity increase in this study could be considered modest, the concentration of the added NPs remained small compared to the overall

Table 2 pHEMA-co-MAA NP samples printed with an Anycubic Photon S 3D printer. The control and all the samples with the NPs were exposed for 25 s and 70 s per layer, respectively

Sample	Surface	Lateral	Dimensions (mm)
Control			$h = 2.17$ $d = 10.04$
PEDOT 0.25×			$h = 2.20$ $d = 10.23$
PEDOT 0.33×			$h = 2.17$ $d = 10.28$
PEDOT 0.5×			$h = 2.2$ $d = 10.19$
PEDOT 1×	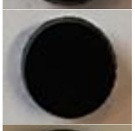		$h = 2.2$ $d = 10.07$
PPy 0.25×	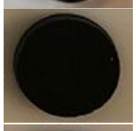		$h = 2.26$ $d = 9.62$
PPy 0.33×	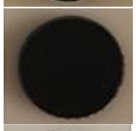		$h = 2.36$ $d = 10.0$
PPy 0.5×			$h = 1.87$ $d = 9.80$
PPy 1×	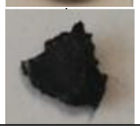		$h =$ N/A $d =$ N/A

pHEMA-co-MAA: poly(2-hydroxyethyl methacrylate-co-methacrylic acid); NP: nanoparticle; 3D: three-dimensional; PEDOT: poly(3,4-ethylene-dioxythiophene); PPy: polypyrrole; N/A: not available

hydrogel system concentration, especially as percolation has not been reached at these NP concentrations [7]. Furthermore, pHEMA has been previously combined with graphene oxide and gelatin for bone tissue engineering, resulting in a conductivity of 1.55×10^{-5} S/cm for 0.75% (mass fraction) graphene oxide concentration [35]. Increasing the conductivity of materials reportedly influences cell growth and proliferation positively, especially in the case of cells of a conductive nature, such as neurons or cardiac cells [15, 16].

pHEMA-co-MAA NP-laden hydrogels swelling properties

The pHEMA-co-MAA NP-laden hydrogel swelling profiles indicated that all samples swelled over 50% after 15 min of immersion in DI water, though samples with lower NP concentrations kept swelling after 30 min of immersion (Fig. 5c). Concerning the PEDOT NP-laden samples, we observed increased swelling degrees from (56.4±3.8)% to (67.9±1.5)% for the 0.25× sample, while that of the 1× sample decreased from (64.0±1.3)% to (54.3±7.0)% within the same 15-min observation period. The trend remained similar in the PPy NP samples, with the PPy 0.25× sample increasing in swelling degree from (64.3±2.6)% to (75.0±3.5)% and the 0.5× sample decreasing from (70.2±3.7)% to (65.1±9.0)%. This could be potentially attributed to the presence of hydrophobic NPs, which inhibited water entry [7]. The control followed the behavior of low-NP-concentration samples, with a swelling degree increasing from (69.3±1.2)% to (70.6±3.5)%, yielding the highest swelling degree. After 30 min, the swelling degree of all samples exhibited the same behavior with a progressively decreasing percentage value. Sample swelling was initially rapid, but then slowly decreased upon reaching about 70% of swelling degree, with equilibrium in the swelling degree established after 96 h.

pHEMA-co-MAA NP-laden hydrogel chemical analysis

The FTIR spectra of the pHEMA-co-MAA NP-laden hydrogel samples (Fig. 6a) show the most important bands of the pHEMA-co-MAA hydrogel as follows: from 3330 to 2872 cm^{-1} indicates the O–H stretching; the peak in 1715 cm^{-1} corresponds to the C=O bond; from 1440 to 1330 cm^{-1} there is O–H bending; the wavelength at 1031 cm^{-1} represents the C–O stretching, and the peak at 911 cm^{-1} is representative of the double bond C=C [36, 37].

As the NP concentrations remained low compared to the overall pHEMA-co-MAA solution concentration, all peaks in the FTIR spectra could be assigned to the pHEMA-co-MAA hydrogel. The FTIR bands for all samples were equal to those of the control with no NPs. The FTIR spectra of the isolated NPs are presented in Fig. 6b, where PEDOT NPs presented the following peaks: peak at 1315 cm^{-1} corresponds to the S=O vibration; 1181 cm^{-1}, 1124 cm^{-1} and 1076 cm^{-1} peaks correspond to the C–O–C bond vibration; the wavelength at 1030 cm^{-1} refers to O–S–O signal and finally the peaks at 965 cm^{-1}, 915 cm^{-1} and 830 cm^{-1} [7, 27, 38] correspond to the C–S bond of the thiophene.

The PPy NPs presented the following peaks: the wavelength at 1545 cm^{-1} corresponds to the C=C bond; 1470

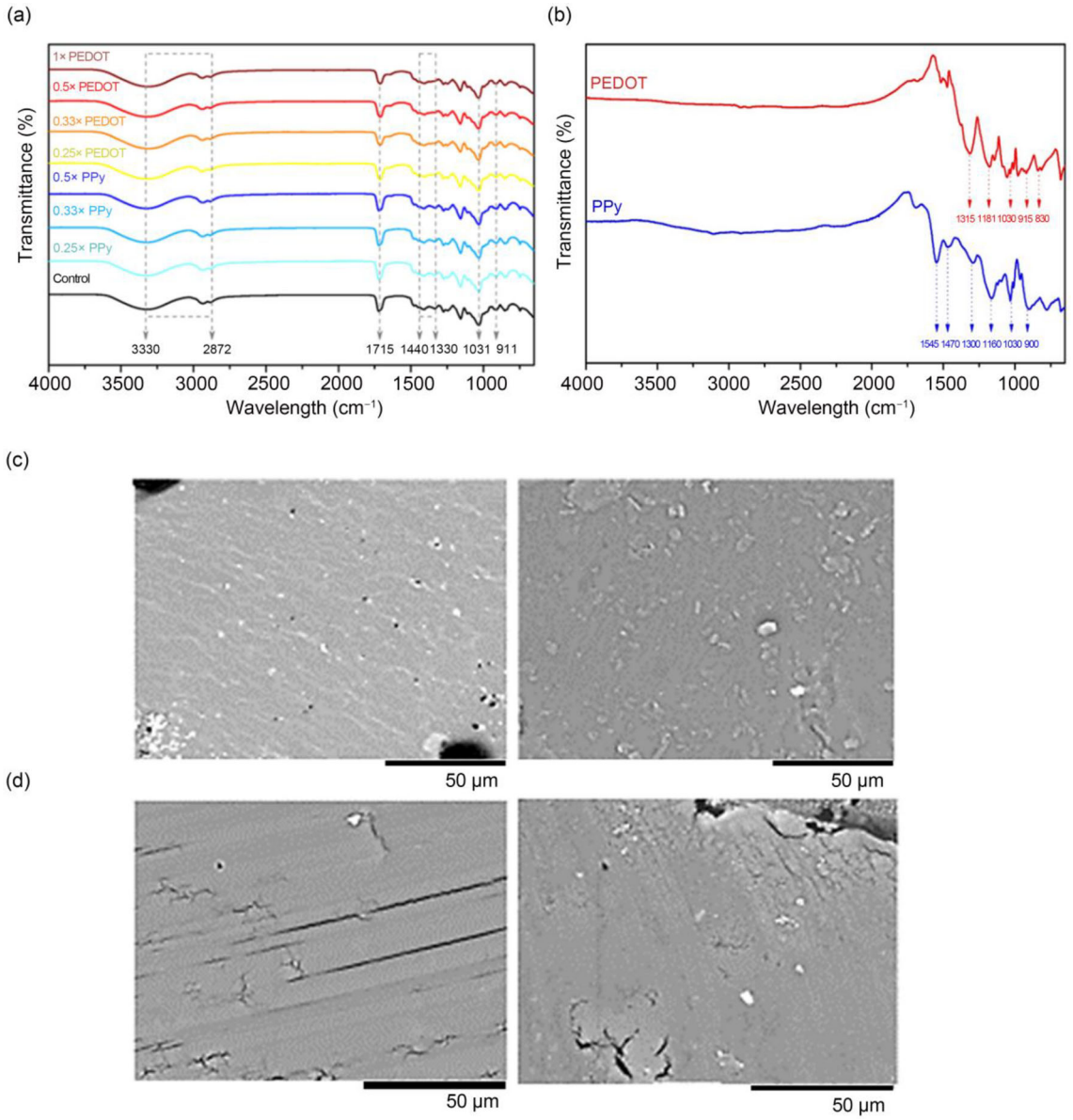

Fig. 6 FTIR analysis of **a** pHEMA-co-MAA NP samples and **b** PEDOT and PPy NPs. **c**, **d** SEM images of the control (left) and a sample with NPs (right): sample **c** surfaces and **d** cross-sections. Scale bar: 50 μm. pHEMA-co-MAA: poly(2-hydroxyethyl methacrylate-co-methacrylic acid); NP: nanoparticle; PEDOT: poly(3,4-ethylene-dioxythiophene); PPy: polypyrrole; SEM: scanning electron microscope

cm^{-1} represents a single bond C–C ring stretching; the peaks at 1300 and 1160 cm^{-1} refer to in-plain vibrations of C–H; the peak at 1030 cm^{-1} corresponds to the plane vibration of C–H and N–H and finally, the wavelength at 900 cm^{-1} is indicative of the deformation vibration of out-plane C–H in the pyrrole ring [20, 39, 40].

pHEMA-co-MAA NP-laden hydrogel morphological properties

SEM analysis was performed on lyophilised samples to observe the hydrogels' morphological features, with the results shown in Figs. 6c and 6d. The surface and cross-sectional images indicate a similar surface pattern with a relatively smooth and flat surface and a lack of porosity, caused by the printing of block constructs. The lack of porosity could be easily altered by changing the printing designs

to allow for the desired porosity in accordance with particular TE needs of 100–500 μm [41], especially when printing with digital light processing (DLP) methods at printing resolutions as low as 50 μm [42].

pHEMA-co-MAA NP-laden hydrogel cytocompatibility assessment in vitro

Visualization of the astrocytes cultured in the presence of pHEMA-co-MAA NP-laden hydrogel media over a 96 h period was conducted by means of LIVE/DEAD staining, with live cells stained green and dead cells stained red (Fig. 7). We observed high-level cell viability in all tested groups. Furthermore, we detected typical spindle-like morphology of the astrocytes with the cells extending to form clusters, indicating that the presence of the hydrogels did not alter healthy cell growth and behavior of the cells. Among all pHEMA-co-MAA NP-laden hydrogel groups, the percentage of live cells was higher than 70%, with the highest values achieved in the PEDOT 1× and PPy 0.25× samples with viabilities of (82.5±1.8)% and (91.9±4.3)%, respectively (Fig. 8a). Decreasing PEDOT NP concentration also decreased the cell viability (e.g., in the PEDOT 0.25× group, the cell viability was (72.7±8.0)%). In contrast, increasing PPy NP concentrations reduced cell viability, with the PPy 0.5× sample yielding cell viability of (71.4±2.1)%. Taken together, the presence of both the PEDOT and PPy NPs positively influenced cell viability compared to the pHEMA-co-MAA hydrogel control with no NPs, which yielded the lowest viability of all the tested samples at (69.2±2.6)%. One-way ANOVA analysis indicated statistical differences between the samples.

Cellular distribution and morphology were also assessed by means of DAPI/Phalloidin staining, as shown in Fig. 7. We cultured the astrocytes in the presence of the pHEMA-co-MAA NP-laden hydrogel media over 96 h, followed by fixation and subsequent DAPI/phalloidin staining to visualize the nuclei and F-actin, respectively. Overall, we observed a similar cellular distribution and morphology of cells to those observed in the LIVE/DEAD analysis, with the cells growing outward from the centered clusters. Quantification of the number of cells using the nuclear staining (Fig. 8b) detected higher viability in the pHEMA-co-MAA NP-laden hydrogel samples than in the pHEMA-co-MAA-only group (e.g., (2282.5±752.7) cells in the PEDOT 0.33× group vs. (1763.75±509.6) cells in the pHEMA-co-MAA-only group). One-way ANOVA indicated no statistical difference between the samples.

Next, using the Alamar Blue proliferation assay, we investigated astrocyte proliferation upon exposure to the pHEMA-co-MAA NP-laden hydrogels. To ensure the absence of cytotoxic leachables from the hydrogels, the indirect contact method was utilized as pHEMA-co-MAA possesses no cell attachment sites. The hydrogels themselves and their constituent NPs are reportedly biocompatible [7, 20, 27]. Using the indirect contact method, we cultured the astrocytes in the presence of pHEMA-co-MAA NP-laden hydrogel-treated cell culture media and measured the cellular fluorescence outputs over a 120 h period (Fig. 8c). Overall, the proliferative ability of the cells increased in all tested samples during the observation, with the PEDOT 0.5× sample yielding the highest value of (70.4±2.7)% at 24 h, though the PEDOT 1× sample displayed a similar proliferation rate of (68.5±4.1)%. When examining the PPy group, the PPy 0.5× group had the highest proliferation rate of (65.2±4.7)%. In general, decreasing NP concentrations reduced the cell proliferative capacity both in the case of PEDOT and PPy (e.g. the PEDOT 0.33× sample resulted in proliferation rate of (60.2±2.6)%). The same trend can also be observed at 72 and 120 h. The pHEMA-co-MAA hydrogels without NPs exhibited lower proliferation rates than heavily NP-laden samples (e.g., (64.8±12.0)% at 24 h). In summary, NP supplementation into the pHEMA-co-MAA hydrogels positively affected cell proliferation and viability. Two-way ANOVA confirmed statistical differences between the sample sets.

pHEMA-co-MAA NP-laden hydrogel antimicrobial assessment

Finally, we assessed the potential antimicrobial properties of the pHEMA-co-MAA NP-laden hydrogels by OD measurements of *S. epidermis*, a common skin commensal bacterial strain. We seeded the bacteria onto the pHEMA-co-MAA NP-laden hydrogels and cultured them for 72 h. In general, both the PEDOT and PPy NP supplementation influenced *S. epidermis* bacterial growth, especially at higher NP concentrations. During the initial 48 h, the OD was below 0.02 for all samples, indicating no exponential bacterial growth in the planktonic phase. When examining the samples at 72 h, bacterial growth was observed. Compared to the pHEMA-co-MAA control with no NPs (OD=0.2±0.06), the PEDOT 1× and PPy 0.5× samples exhibited ODs of 0.13±0.04 and 0.19±0.06, respectively. ANOVA analysis indicated statistical differences between the samples at 72 h. In all groups, the OD values remained below 0.3 at 72 h. Materials with measured OD values above 0.2 are generally considered to possess biofilm-forming abilities [43–46]. This could indicate that the presence of pHEMA-co-MAA NP-laden hydrogels does not favor bacterial growth during the planktonic phase of the initial 48 h of incubation, potentially indicating the antimicrobial properties of these materials. Further evaluations should fully support this statement.

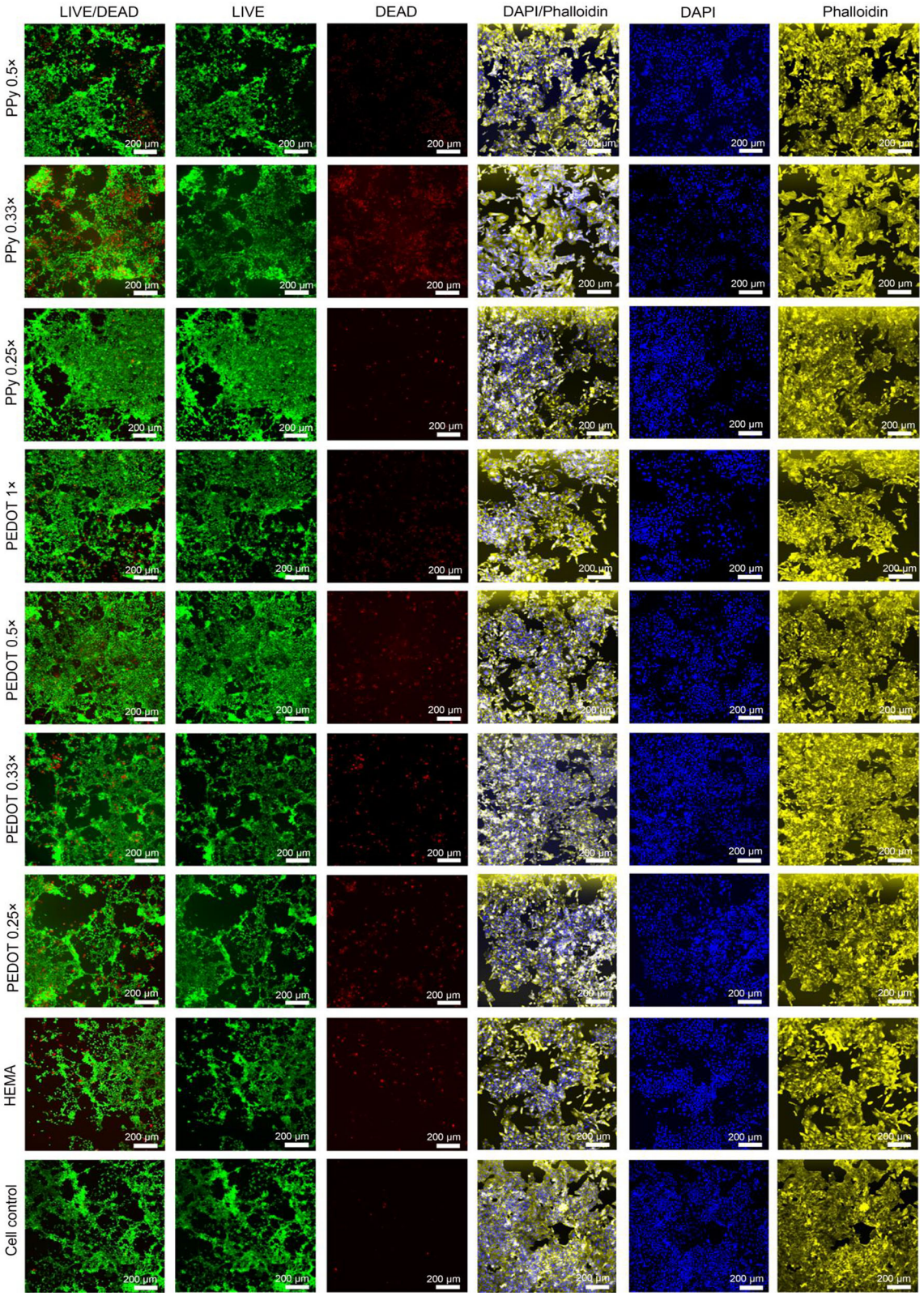

Fig. 7 Viable astrocytes when cultured in media treated with pHEMA-co-MAA NP hydrogels, exhibiting optimal cellular morphology in vitro. LIVE/DEAD and DAPI and phalloidin staining of astrocytes cultured for 96 h in pHEMA-co-MAA NP sample-containing media. Scale bar: 200 μm. pHEMA-co-MAA: poly(2-hydroxyethyl methacrylate-co-methacrylic acid); NP: nanoparticle; PEDOT: poly(3,4-ethylenedioxythiophene); PPy: polypyrrole; HEMA: hydroxyethyl methacrylate; DAPI: 4',6-diamidino-2-phenylindole

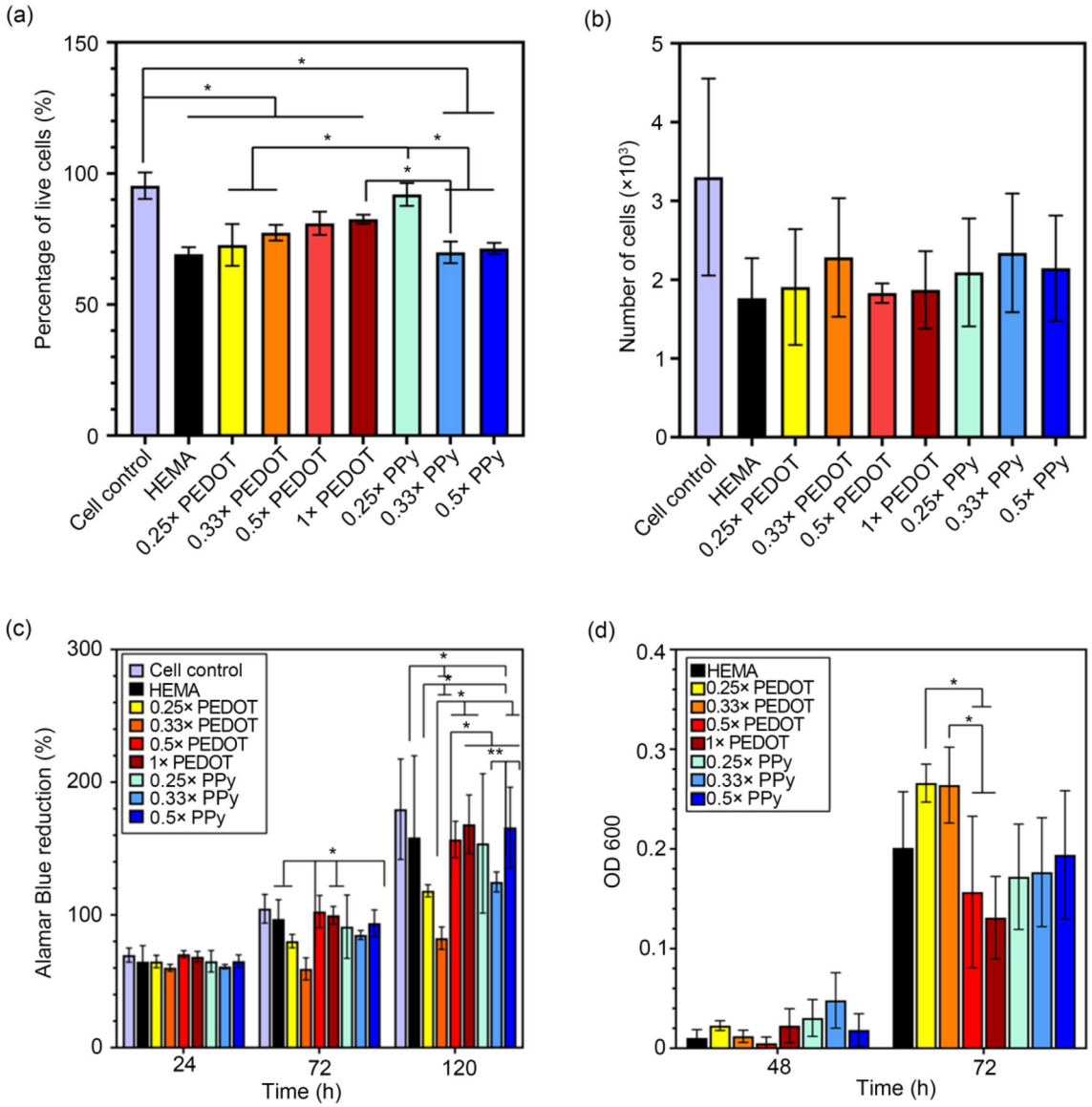

Fig. 8 **a** LIVE/DEAD assay-based cell viability quantification, analyzed using ImageJ from Fig. 7; $^{*}p<0.05$ ($n=3$, mean±SD). **b** DAPI/phalloidin-stained astrocyte number quantification, analyzed using ImageJ from Fig. 7; $^{*}p<0.05$ ($n=3$, mean±SD). **c** Alamar Blue proliferation assay-based cytotoxicity assessment in astrocytes cultured for 120 h in pHEMA-co-MAA NP hydrogel-treated media. **d** OD measurement of *S. epidermis* bacteria cultured on the surface of pHEMA-co-MAA NP hydrogels for 72 h; $^{*}p<0.05$ ($n=3$, mean±SD). SD: standard deviation; pHEMA-co-MAA: poly(2-hydroxyethyl methacrylate-co-methacrylic acid); NP: nanoparticle; OD: optical density; PEDOT: poly(3,4-ethylene-dioxythiophene); PPy: polypyrrole; HEMA: hydroxyethyl methacrylate; DAPI: 4',6-diamidino-2-phenylindole

Conclusions

In this study, we successfully incorporated PEDOT and PPy NPs into a pHEMA-co-MAA hydrogel system and performed 3D printing with in situ photopolymerization. Blue/black NP supplementation affected UV penetration capacities and thereby affected hydrogel crosslinking, with longer curing times required for crosslinking samples with higher NP concentrations. This was particularly observed for PPy NPs with a higher UV absorbance than PEDOT NPs. The physicochemical characterization demonstrated that the pHEMA-co-MAA NP-laden hydrogels possessed excellent mechanical properties between 450 and 550 kPa, with swelling profiles reaching an equilibrium within 30 min. Conductive NP incorporation increased the hydrogel electrical conductivity to $(5.10\pm0.37)\times10^{-7}$ S/cm. Prior to UV light exposure, the pHEMA-co-MAA NP-laden hydrogels exhibited shear thinning behavior, rendering them ideal for

printing applications. In vitro biocompatibility studies indicated that NP supplementation into the pHEMA-co-MAA hydrogel system favors cell growth and viability. Our antimicrobial studies implied that the pHEMA-co-MAA NP-laden hydrogel system influenced *S. epidermis* bacterial growth in the initial 48 h. In summary, the newly synthesized pHEMA-co-MAA NP-laden hydrogels presented in this study hold promising potential for various electroactive TE strategies.

Acknowledgements This publication has emanated from research conducted with the financial support of Science Foundation Ireland under the SFI Research Infrastructure Programme (21/RI/9831). The authors would like to thank the funding provided by the Irish Research Council through the Irish Research Council Enterprise Partnership Scheme with Johnson and Johnson (EPSPG/2020/78). Illustrations in Figs. 1 and 2 were created using BioRender.

Author contributions Data curation: SDN, AS (Aleksandra Serafin), AK, and AS (Achim Schmalenberger); writing of the manuscript: SDN, AS (Aleksandra Serafin), and MNC; supervision: AS (Aleksandra Serafin), AS (Achim Schmalenberger), JJEM, and MNC; revision of the manuscript: AS (Aleksandra Serafin), AK, AS (Achim Schmalenberger), JJEM, and MNC; funding acquisition: AS (Aleksandra Serafin) and MNC.

Funding Open Access funding provided by the IReL Consortium.

Data availability The datasets used and analyzed in this study are available from the corresponding author upon reasonable request.

Declarations

Conflict of interest The authors declare that they have no conflict of interest.

Ethical approval This article does not contain any studies with human or animal subjects performed by any of the authors.

References

1. Starzl TE (2000) History of clinical transplantation. World J Surg 24(7):759–782. https://doi.org/10.1007/s002680010124
2. Gulsen D, Chauhan A (2005) Dispersion of microemulsion drops in HEMA hydrogel: a potential ophthalmic drug delivery vehicle. Int J Pharm 292(1):95–117. https://doi.org/10.1016/j.ijpharm.2004.11.033
3. Geckil H, Xu F, Zhang XH et al (2010) Engineering hydrogels as extracellular matrix mimics. Nanomedicine 5(3):469–484. https://doi.org/10.2217/nnm.10.12
4. Montheard JP, Chatzopoulos M, Chappard D (1992) 2-hydroxyethyl methacrylate (HEMA): chemical properties and applications in biomedical fields. J Macromol Sci Part C 32(1):1–34. https://doi.org/10.1080/15321799208018377
5. Fornasiero F, Krull F, Radke CJ et al (2004) Diffusivity of water through a HEMA-based soft contact lens. Fluid Phase Equilib 228–229:269–273. https://doi.org/10.1016/j.fluid.2004.08.020
6. Efron N, Brennan NA, Chalmers RL et al (2020) Thirty years of "quiet eye" with etafilcon A contact lenses. Cont Lens Anterior Eye 43(3):285–297. https://doi.org/10.1016/j.clae.2020.03.015
7. Serafin A, Rubio MC, Carsi M et al (2022) Electroconductive PEDOT nanoparticle integrated scaffolds for spinal cord tissue repair. Biomater Res 26(1):63. https://doi.org/10.1186/s40824-022-00310-5
8. An J, Teoh JEM, Suntornnond R et al (2015) Design and 3D printing of scaffolds and tissues. Engineering 1(2):261–268. https://doi.org/10.15302/J-ENG-2015061
9. Askari M, Afzali Naniz M, Kouhi M et al (2021) Recent progress in extrusion 3D bioprinting of hydrogel biomaterials for tissue regeneration: a comprehensive review with focus on advanced fabrication techniques. Biomater Sci 9(3):535–573. https://doi.org/10.1039/d0bm00973c
10. Sahafnejad-Mohammadi I, Rahmati S, Najmoddin N et al (2023) Biomimetic polycaprolactone-graphene oxide composites for 3D printing bone scaffolds. Macromol Mater Eng 308(5):2200558. https://doi.org/10.1002/mame.202200558
11. Noroozi R, Tatar F, Zolfagharian A et al (2022) Additively manufactured multi-morphology bone-like porous scaffolds: experiments and micro-computed tomography-based finite element modeling approaches. Int J Bioprint 8(3):40–56. https://doi.org/10.18063/ijb.v8i3.556
12. Schuldt SJ, Jagoda JA, Hoisington AJ et al (2021) A systematic review and analysis of the viability of 3D-printed construction in remote environments. Automat Constr 125:103642. https://doi.org/10.1016/j.autcon.2021.103642
13. Steel EM, Azar JY, Sundararaghavan HG (2020) Electrospun hyaluronic acid-carbon nanotube nanofibers for neural engineering. Materialia 9:100581. https://doi.org/10.1016/j.mtla.2019.100581
14. Chen MQ, Xie XY, Hollis Whittington R et al (2008) Cardiac differentiation of embryonic stem cells with point-source electrical stimulation. In: 30th Annual International Conference of the IEEE Engineering in Medicine and Biology Society, p.1729–1732. https://doi.org/10.1109/IEMBS.2008.4649510
15. Kuzmenko V, Kalogeropoulos T, Thunberg J et al (2016) Enhanced growth of neural networks on conductive cellulose-derived nanofibrous scaffolds. Mater Sci Eng C Mater Biol Appl 58:14–23. https://doi.org/10.1016/j.msec.2015.08.012
16. McCaig CD, Rajnicek AM, Song B et al (2005) Controlling cell behavior electrically: current views and future potential. Physiol Rev 85(3):943–978. https://doi.org/10.1152/physrev.00020.2004
17. Edwards SL, Werkmeister JA, Ramshaw JA (2009) Carbon nanotubes in scaffolds for tissue engineering. Expert Rev Med Devices 6(5):499–505. https://doi.org/10.1586/erd.09.29
18. Noroozi R, Shamekhi MA, Mahmoudi R et al (2022) In vitro static and dynamic cell culture study of novel bone scaffolds based on 3D-printed PLA and cell-laden alginate hydrogel. Biomed Mater 17(4):045024. https://doi.org/10.1088/1748-605X/ac7308
19. Serafin A, Murphy C, Rubio MC et al (2021) Printable alginate/gelatin hydrogel reinforced with carbon nanofibers as electrically conductive scaffolds for tissue engineering. Mater Sci Eng C 122:111927. https://doi.org/10.1016/j.msec.2021.111927

20. Serafin A, Culebras M, Oliveira JM et al (2023) 3D printable electroconductive gelatin-hyaluronic acid materials containing polypyrrole nanoparticles for electroactive tissue engineering. Adv Compos Hybrid Mater 6(3):109. https://doi.org/10.1007/s42114-023-00665-w
21. Spencer AR, Primbetova A, Koppes AN et al (2018) Electroconductive gelatin methacryloyl-PEDOT:PSS composite hydrogels: design, synthesis, and properties. ACS Biomater Sci Eng 4(5):1558–1567. https://doi.org/10.1021/acsbiomaterials.8b00135
22. Song E, Choi JW (2013) Conducting polyaniline nanowire and its applications in chemiresistive sensing. Nanomaterials 3(3):498–523. https://doi.org/10.3390/nano3030498
23. Mantione D, del Agua I, Sanchez-Sanchez A et al (2017) Poly(3,4-ethylenedioxythiophene) (PEDOT) derivatives: innovative conductive polymers for bioelectronics. Polymers 9(8):354. https://doi.org/10.3390/polym9080354
24. Boni R, Ali A, Shavandi A et al (2018) Current and novel polymeric biomaterials for neural tissue engineering. J Biomed Sci 25(1):90. https://doi.org/10.1186/s12929-018-0491-8
25. Chiang CW, Chuang EY (2019) Biofunctional core-shell polypyrrole-polyethylenimine nanocomplex for a locally sustained photothermal with reactive oxygen species enhanced therapeutic effect against lung cancer. Int J Nanomed 14:1575–1585. https://doi.org/10.2147/IJN.S163299
26. Saleemi MA, Hosseini Fouladi M, Yong PVC et al (2021) Toxicity of carbon nanotubes: molecular mechanisms, signaling cascades, and remedies in biomedical applications. Chem Res Toxicol 34(1):24–46. https://doi.org/10.1021/acs.chemrestox.0c00172
27. Escobar A, Serafin A, Carvalho MR et al (2023) Electroconductive poly(3,4-ethylenedioxythiophene) (PEDOT) nanoparticle-loaded silk fibroin biocomposite conduits for peripheral nerve regeneration. Adv Compos Hybrid Mater 6(3):118. https://doi.org/10.1007/s42114-023-00689-2
28. Yang Y, Deng H, Fu Q (2020) Recent progress on PEDOT:PSS based polymer blends and composites for flexible electronics and thermoelectric devices. Mater Chem Front 4(11):130–152. https://doi.org/10.1039/D0QM00308E
29. Culebras M, Byun Y, Jang J et al (2023) Nanostructured PEDOT-based multilayer thin films with high thermoelectric performances. Appl Surf Sci 615:156432. https://doi.org/10.1016/j.apsusc.2023.156432
30. Shannon A, Guttridge C, O'Sullivan A et al (2024) Comparing digital light processing and stereolithography vat polymerization technologies for antimicrobial 3D printing using silver oxide as an antimicrobial filler. J Appl Polym Sci 141(12):55122. https://doi.org/10.1002/app.55122
31. Şarkaya K, Çadırcı M, Çetin K et al (2023) PHEMA/PPy cytocompatible conductive cryogels: one-pot synthesis, characterization, and electrical properties. Mater Today Commun 35:105791. https://doi.org/10.1016/j.mtcomm.2023.105791
32. Arslantunali D, Budak G, Hasirci V (2014) Multiwalled CNT-pHEMA composite conduit for peripheral nerve repair. J Biomed Mater Res Part A 102(3):828–841. https://doi.org/10.1002/jbm.a.34727
33. Allijn I, Ribeiro M, Poot A et al (2020) Membranes for modelling cardiac tissue stiffness in vitro based on poly(trimethylene carbonate) and poly(ethylene glycol) polymers. Membranes 10(10):274. https://doi.org/10.3390/membranes10100274
34. Karimi A, Shojaei A (2017) Measurement of the mechanical properties of the human kidney. IRBM 38(5):292–297. https://doi.org/10.1016/j.irbm.2017.08.001
35. Tabatabaee S, Baheiraei N, Salehnia M (2022) Fabrication and characterization of PHEMA-gelatin scaffold enriched with graphene oxide for bone tissue engineering. J Orthop Surg Res 17(1):216. https://doi.org/10.1186/s13018-022-03122-4
36. Vargün E, Usanmaz A (2010) Degradation of poly(2-hydroxyethyl methacrylate) obtained by radiation in aqueous solution. J Macromol Sci Part A 47(9):882–891. https://doi.org/10.1080/10601325.2010.501304
37. Rashid H, Ahmad M, Minhas MU et al (2015) Synthesis and characterization of poly(hydroxyethyl methacrylate-co-methacrylic acid) cross linked polymeric network for the delivery of analgesic agent. J Chem Soc Pakistan 37(5):999–1007
38. Liu YZ, Sun D, Askari S et al (2015) Enhanced dispersion of TiO_2 nanoparticles in a TiO_2/PEDOT:PSS hybrid nanocomposite via plasma-liquid interactions. Sci Rep 5(1):15765. https://doi.org/10.1038/srep15765
39. Liu Y, Chu Y, Yang LK (2006) Adjusting the inner-structure of polypyrrole nanoparticles through microemulsion polymerization. Mater Chem Phys 98(2):304–308. https://doi.org/10.1016/j.matchemphys.2005.09.025
40. Chen Y, Kang GY, Xu H et al (2016) Two composites based on $CoMoO_4$ nanorods and PPy nanoparticles: fabrication, structure and electrochemical properties. Synth Met 215:50–55. https://doi.org/10.1016/j.synthmet.2016.02.006
41. Murphy CM, O'Brien FJ (2010) Understanding the effect of mean pore size on cell activity in collagen-glycosaminoglycan scaffolds. Cell Adh Migr 4(3):377–381. https://doi.org/10.4161/cam.4.3.11747
42. Waheed S, Cabot JM, Macdonald NP et al (2016) 3D printed microfluidic devices: enablers and barriers. Lab Chip 16(11):1993–2013. https://doi.org/10.1039/c6lc00284f
43. Zamboni F, Wong CK, Collins MN (2023) Hyaluronic acid association with bacterial, fungal and viral infections: can hyaluronic acid be used as an antimicrobial polymer for biomedical and pharmaceutical applications? Bioact Mater 19:458–473. https://doi.org/10.1016/j.bioactmat.2022.04.023
44. Flynn J, Culebras M, Collins MN et al (2022) The impact of varying dextran oxidation levels on the inhibitory activity of a bacteriocin loaded injectable hydrogel. Drug Deliv Transl Res 13(1):308–319. https://doi.org/10.1007/s13346-022-01201-x
45. Zamboni F, Okoroafor C, Ryan MP et al (2021) On the bacteriostatic activity of hyaluronic acid composite films. Carbohyd Polym 260:117803. https://doi.org/10.1016/j.carbpol.2021.117803
46. Flynn J, Durack E, Collins MN et al (2020) Tuning the strength and swelling of an injectable polysaccharide hydrogel and the subsequent release of a broad spectrum bacteriocin, nisin A. J Mater Chem B 8(18):429–438. https://doi.org/10.1039/d0tb00169d